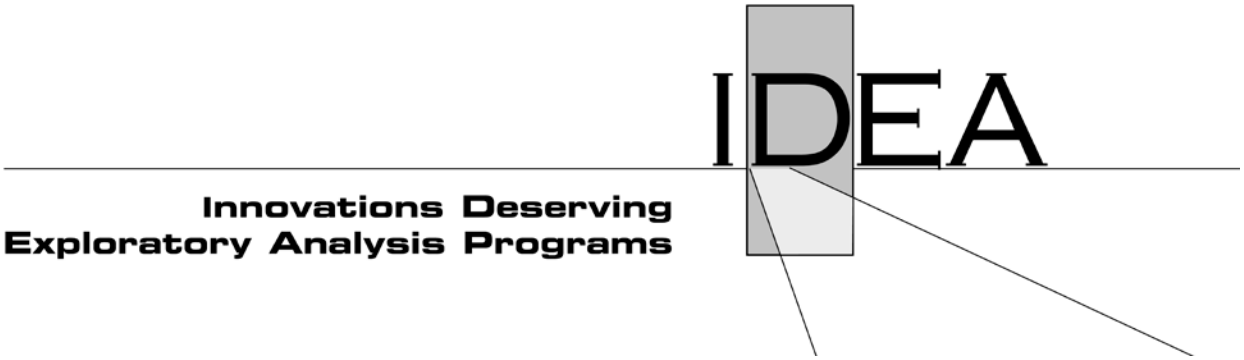

Rail Safety IDEA Program

Vibration-based Longitudinal Rail Stress Estimation Exploiting Acoustic Measurement and Machine Learning

Final Report for
Rail Safety IDEA Project 41

Prepared by:
John S. Popovics
Marcus S. Dersch
University of Illinois Urbana-Champaign

Xuan Zhu
University of Utah

October 2020

TRB TRANSPORTATION RESEARCH BOARD
The National Academies of
SCIENCES · ENGINEERING · MEDICINE

Innovations Deserving Exploratory Analysis (IDEA) Programs Managed by the Transportation Research Board

This IDEA project was funded by the Rail Safety IDEA Program.

The TRB currently manages the following three IDEA programs:

- The NCHRP IDEA Program, which focuses on advances in the design, construction, and maintenance of highway systems, is funded by American Association of State Highway and Transportation Officials (AASHTO) as part of the National Cooperative Highway Research Program (NCHRP).
- The Rail Safety IDEA Program currently focuses on innovative approaches for improving railroad safety or performance. The program is currently funded by the Federal Railroad Administration (FRA). The program was previously jointly funded by the Federal Motor Carrier Safety Administration (FMCSA) and the FRA.
- The Transit IDEA Program, which supports development and testing of innovative concepts and methods for advancing transit practice, is funded by the Federal Transit Administration (FTA) as part of the Transit Cooperative Research Program (TCRP).

Management of the three IDEA programs is coordinated to promote the development and testing of innovative concepts, methods, and technologies.

For information on the IDEA programs, check the IDEA website (www.trb.org/idea). For questions, contact the IDEA programs office by telephone at (202) 334-3310.

IDEA Programs
Transportation Research Board
500 Fifth Street, NW
Washington, DC 20001

Vibration-based Longitudinal Rail Stress Estimation Exploiting Acoustic Measurement and Machine Learning

IDEA Program Final Report

For the period *April/2019* through *July/2020*

Contract Number Rail Safety 41

Prepared for the IDEA Program

Transportation Research Board

National Academies of Sciences, Engineering, and Medicine

John S. Popovics, PhD, PE, Professor
Marcus S. Dersch, PE, Principal Research Engineer
Department of Civil and Environmental Engineering
University of Illinois Urbana-Champaign

Xuan Zhu, PhD, Assistant Professor
Department of Civil and Environmental Engineering
University of Utah
October 2020

Acknowledgments

This project was supported by the National Academies' Transportation Research Board (TRB) IDEA program. The Principal Investigators express sincere thanks to the Expert Review Panel: Mr. Conrad Ruppert, Mr. William Dombrow, Prof. Francesco Lanza di Scalea (University of California, San Diego), and Prof. Yongchao Yang (Michigan Technological University) for their participation, guidance, and helpful comments during the course of this project. The PIs also extend special thanks to the IDEA program coordinator, Dr. Velvet Fitzpatrick, for her support, guidance, and timely suggestions.

The PIs are deeply thankful to John Mazza from Instrumentation Service, Inc. for his technical support on rail instrumentation, and Andrew Kish from Kandrew Inc. Consulting Services and Harold Harrison from Salient Systems, Inc. for their advice on rail neutral temperature. This research and development project required strong contributions from our team; the PIs truly appreciate the time and effort of the following individuals: Mr. Chi-luen Huang (UIUC), Mr. Sangmin Lee (UIUC), and Mr. Yuning Wu (University of Utah).

Glossary

AREMA	American Railway Engineering and Maintenance-of-Way Association
BNSF	BNSF Railway Company
CWR	Continuous Welded Rail
FEM	Finite Element Model
FRA	Federal Railroad Administration
NN	Neural Network
RNT	Rail Neutral Temperature
ZGV	Zero-Group Velocity

Table of Contents

List of Figures

Investigator Profile

Principal Investigator: John S. Popovics holds B.S. and M.S. degrees (Drexel University 1988 and 1990, respectively) in civil engineering, and a Ph.D. (The Pennsylvania State University 1994) in engineering science and mechanics. He has been on the faculty of the Department of Civil and Environmental Engineering at the University of Illinois since January 2002 and currently holds the rank of Professor and the title of Caterpillar Faculty Scholar. He has also held the positions of Research Assistant Professor at Northwestern University, Assistant Professor at Drexel University, Guest Scientist at the German Federal Materials Research Institute (BAM-Berlin), Visiting Professor at the Polytechnic University of Valencia in Spain, and Visiting Researcher at the Laboratoire Centrale des Pont et Chaussées (LCPC) in France. Dr. Popovics is a member of the American Society of Civil Engineers, and he is a named Fellow of the American Concrete Institute and the American Society for Nondestructive Testing. He serves as an associate editor for the Journal of Nondestructive Testing.

Co-Principal Investigator: Xuan Zhu holds B.S. in mechanical engineering from Beijing University of Aeronautics and Astronautics, an M.S. in civil engineering from the University of Pittsburgh, and a Ph.D. in structural engineering from the University of California, San Diego. He currently serves as an Assistant Professor in the Civil and Environmental Engineering Department at the University of Utah. Dr. Zhu has been conducting research that spans the breadth of experimental, theoretical, and numerical approaches in the fields of NDT and experimental mechanics, along with their applications in transportation and energy infrastructure. He received many awards for academic excellence, such as CALRA Fellowship, Dissertation Fellowship, and NSF Scholarship. He also serves as a reviewer for top international journals in his research field. Dr. Zhu is a member of the American Society for Nondestructive Testing and the American Society of Mechanical Engineers.

Co-Principal Investigator: Marcus Dersch obtained his bachelor's degree in civil engineering from the University of Illinois at Urbana-Champaign in 2009, during which time he completed research in railroad engineering focusing on fouled railroad ballast performance. During the summer of 2008, he worked for Union Pacific Railroad as an engineering intern. After obtaining his bachelor's degree, he attended the University of Illinois at Urbana-Champaign to obtain a master's in civil engineering, concentrating and completing research in railroad engineering focusing on ballast performance improvement. He graduated in December of 2010 and began working for the University of Illinois in the Rail Transportation and Engineering Center. Mr. Dersch has research interests in the areas of railroad civil engineering, specifically infrastructure research related to concrete railway crosstie and fastener design and railroad ballast performance.

Executive Summary

The mission of this IDEA project is to serve the rail industry by increasing safety and improving infrastructure reliability by minimizing the risks of rail track buckling. The proposed work aims to address a major rail industry challenge – predicting the stress state of rail, considering the rail neutral temperature (RNT), in a practical, accurate, and effective manner. Such capability would represent a breakthrough in rail monitoring technology. The research team developed and implemented an approach that exploits contactless acoustic sensing, finite element modeling (FEM), and machine learning to estimate RNT using vibration data without disturbing track structure or using additional knowledge from prior baseline measurements. The overall framework of the research team's approach is illustrated in Figure 1. This study is composed of three key components: data collection at a revenue-service line to ensure the proposed sensing technology can function in the field, finite element modeling to interpret field observations and understand the behavior of track vibration characteristics, and machine learning algorithms to establish an input-output relationship between track vibration signatures and *in-situ* RNT.

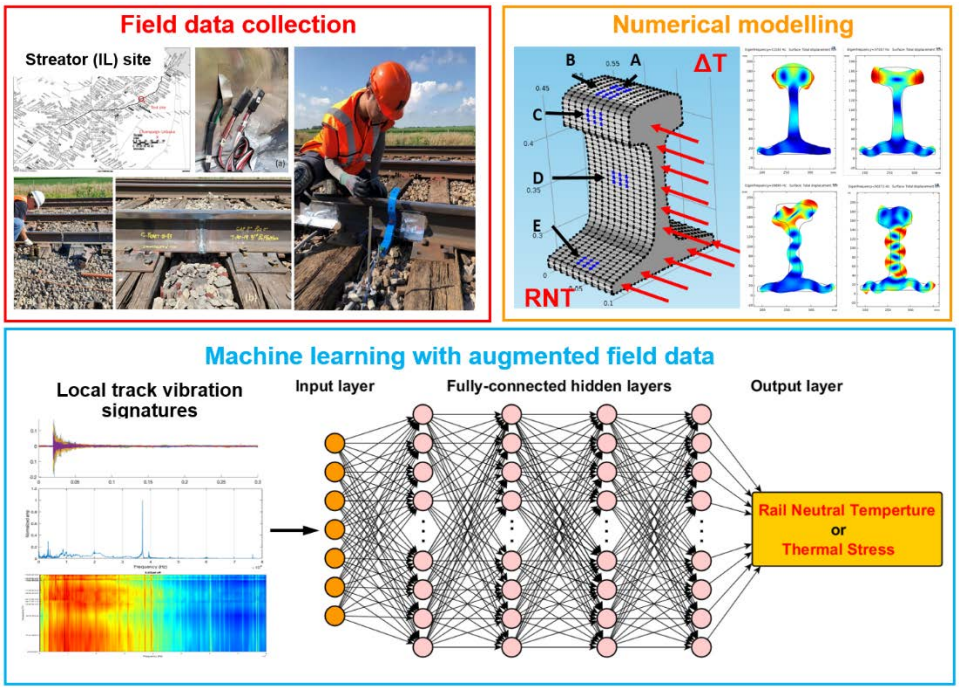

Figure 1: Illustration of the proposed IDEA research approach using rail vibration data that is affected by stress condition and RNT

The tasks in this project were divided into two stages: Stage I and II. The objective of Stage I was to collect track vibration data in a realistic field environment covering a wide range of rail temperature, and thereby thermal stress conditions. The data collected in Stage I was used to build up training data for the Stage II effort. During Stage I, the team

designed and fabricated fixtures for field data collection, and coordinated with the rail partner to establish an instrumented field site that provides continuous rail temperature, axial rail strain, axial rail load, and RNT data on a heavily used revenue-service line in the state of Illinois. Track vibration data were collected over a wide range of temperatures throughout each day during six field trips to the test site. The acoustic vibration test data prove that consistent high-quality signals can be obtained in the frequency range of 20 to 80 kHz. The high-frequency range is desirable because our preliminary results show that rail vibrations in this frequency range are not disrupted by variations in track substructure and foundation.

Stage II activities focused on the development of FEM and machine learning algorithms for RNT prediction using the field-collected and FEM data. Using FEM tools, the behavior of high-frequency rail track vibration was predicted under mechanical and thermal loads, and FEM predictions of resonance frequency were within 0.1% of those collected in the field. Considering the FEM simulation, field vibration data, and ground-truth rail stress and temperature data, the team demonstrated that several specific vibration modes of the rail are affected by thermal stress changes and RNT. Using FEM frequency data from these specific modes under the influence of thermal load, a neural network was designed to predict RNT. The results from the neural network demonstrate that it is feasible to predict RNT using the identified high-frequency modes; the system performance with field data indicates that the proposed framework can support RNT prediction within ±5.5ºC (±9.9ºF) when measurement/model noise is low.

IDEA Product

Safety is of principal concern of the railway industry, and track alignment irregularities can pose risks to the safe operation of trains. According to Federal Railroad Administration (FRA) safety statistics for track-related train accidents, "track alignment irregularities (buckled/sun kink)" are the second leading cause of train accidents, in terms of reportable damage: $131,903,010 reportable damage considering 241 derailments out of 244 accidents occurring between January 2007 and December 2017. The high derailment rate and the potential destructive social and economic impact make track alignment irregularities a high priority issue for the railroad industry.

Rail neutral temperature is defined as the rail temperature at which the longitudinal stress in the rail is zero. Most modern railways use continuous welded rail (CWR), which supports higher transport speeds, provides less friction, and requires less maintenance. It is essential to monitor RNT considering the absence of expansion joints in the rail can lead to track alignment irregularities, possible thermal buckling and fracture. Effective management of RNT remains a long-standing challenge because accurate measurement of in-situ RNT is difficult to obtain in a real-world field environment.

This project developed new concepts and technologies for on-site RNT measurement, combining contactless acoustic vibration sensing and machine learning approaches. The overall project objective is to develop a framework that exploits track vibration and machine learning for RNT estimation on CWR structures. The project scope detail includes (i) to design and develop data acquisition systems for rail track vibrational data collection; (ii) to collect data in a representative real-world field test site with rail temperature and RNT measurements; (iii) to implement machine learning algorithms for RNT prediction; and (iv) to understand advantages and limitations of the developed framework. The proposed testing and analysis approaches feature the following attributes:

- No modification to track structrues - unfastening or unclipping of rail is not needed;
- Real-world data – the research team collects unique high-frequency track vibration data from an instrumented site on a revenue-service line using acoustic non-destructive and non-disrupting sensing technology;
- Numerical simulation –computer models are established to simulate complex track vibration behavior, focusing on cross-sectional modes, and thus enabling deeper understanding and broadened vibration data pool to study real world conditions (e.g. effects of rail wear);
- Advanced data analysis – a machine learning algorithm is developed to predict RNT yet minimize the influences from rail temperature and continuously evolving support and substructure conditions;
- Potential for in-motion RNT measurement - the sensing approach potentially supports a continuous and in-motion RNT measurement through contactless sensing, thereby offering data redundancy to build up statistical confidence.

Concept and Innovation

Concept of application

In this study, we aim to develop new technology for on-site RNT measurement combining acoustic vibration sensing and machine learning technologies. We hypothesize that recent advances in machine learning, e.g., data-driven models backed by neural networks (NN), provide a platform from which useful information about rail stress or RNT can be extracted from a complex and rich data set. Such a system would predict rail stress state or RNT in situ and in real-time and, with further development, could rapidly assess a large inspection area once deployed on a moving platform enabled by contactless sensors. The development of such machine learning models, however, hinges on the ability to collect rail temperature and ground-truth RNT data with which to train the models; these ground-truth data will be provided by a unique collaboration with our industrial partner, BNSF Railway. Upon successful completion of the proposed work, the approach would provide reliable RNT prediction, thus enabling monitoring capability not supported by existing technologies.

Potential payoff for practice

The mission of this project is to serve the rail industry by increasing safety, improving infrastructure reliability, and minimizing the risks of track alignment problems; this is of great interest to the rail industry. Accurate and practical *in-situ* RNT measurement is needed to achieve this objective. Currently employed RNT measurement technology, for example, the VERSE method *(1)*, provides accurate measurements but is time-consuming, labor-intensive, inefficient for a wood tie/cut spike track, and not appropriate for ubiquitous and autonomous measurement. Furthermore, VERSE must be applied when the rail is in a tensile state of stress, which is not applicable for operations during hot weather. Thus, a new technological development that provides accurate and more practical measurement would have a notable payoff for practice. The most important payoffs of our proposed technology and approach include (i) it does not require modification of track structures; (ii) its sensing configuration is simple, robust, and does not involve any hazardous phenomena for humans; and (iii) it analyzes vibrational data using FEM-assist machine learning algorithms, which eliminates the need for reference measurements and reduces influences from varying tie, clip/fastener, and sub-base conditions.

Transfer to practice

Our approach brings promise for effective implementation because the work is supported by in-service rail measurements and knowledge of true rail stress and temperature data. The latter point represents a unique and important aspect of the work, which is enabled through the close cooperation with our rail industry partner BNSF Railway. We maintained regular communication with our technical contact at BNSF, and

we aim to continue this in the future to increase the likelihood that the technology will eventually be implemented in the rail industry. Furthermore, our close partnership with the rail research group at UIUC (RailTEC) helps chances of the technology being implemented in practice because of their extensive history and collaboration with the rail industry.

Investigation

Stage 1: Laboratory and field data collection using contactless sensing

Task 1: Optimize vibrational test configuration

In preparation for laboratory and field testing, the team optimized the vibrational test configuration, and identified the optimal excitation-sensing configuration. A testing configuration and data acquisition system were developed to carry out excitation and contactless sensing on a CWR. A 10 mm-diameter steel sphere was used as an impulse source to introduce vibrational resonances in rail structures. This source was selected because it provides mechanical energy across a sufficiently wide range of frequencies, at least 40 kHz. A polarized condenser microphone (PCB Piezotronics) was used to collect vibration responses of the rail. To capture responses covering a broad range of vibration modes, five locations (A-E) around the rail profile were defined, including three on the rail head (positions A, B, and C), one at the rail web (D), and one on the rail foot (E), as shown in Figure 2(a). Test configurations with all combinations of impact/sensing locations were considered. Moreover, to facilitate field data collection, a sensor holding arm was designed and constructed using a 3-D printer. The holding arm keeps the microphone at proper test positions based on the contours of AREMA 132RE and 136RE rail geometries, as shown in Figure 2(b-d). This holding arm will reduce measurement time by maintaining proper sensor positioning and orientation.

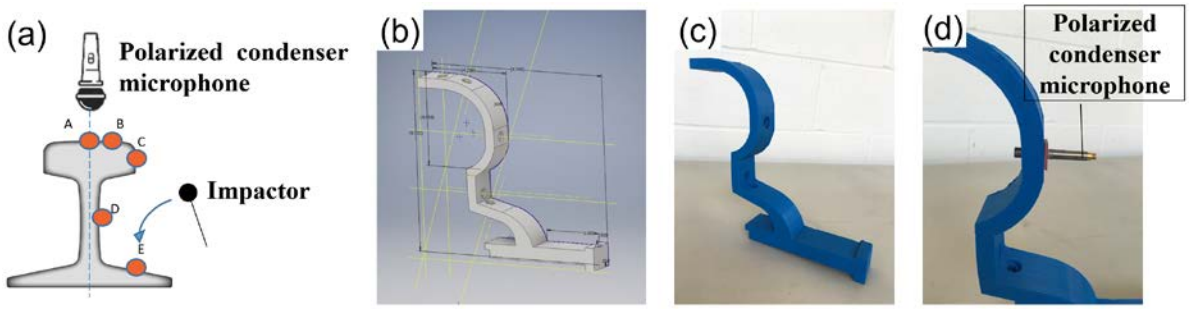

Figure 2: (a) Acoustic monitoring test configurations with 5 impact/sensing locations. Microphone holding arm: (b) design of the holder; (c) 3-D printed holder; (d) holding arm accommodating the condenser microphone

Task 2: Laboratory verification of utility of vibration approach to measure rail stress

To verify system performance and its sensitivities to stress and temperature, rail track vibrational data was collected in the laboratory using two test configurations: (i) a stepwise incremental uniaxial loading conditions at constant rail temperature; and (ii) an incremental rail temperature while the rail sample is free-to-expand.

To investigate the axial load effect, vibrational responses of a short piece of AREMA 132RE rail were studied when subjected to levels of compressive loads. The load was increased from zero to a maximum of 100 MPa in 9 steps, and the sample was unloaded

following the same path. The strain was monitored with strain gauges installed along the neutral axis on the web. The test configuration and loading path are shown in Figure 3(a) and (b), respectively. At each load level, vibration data was collected using all the combinations of test configurations described in Task 1. Generally, all the resonance frequencies shift towards higher frequencies with increasingly compressive loads, as shown in Figure 4(a). Furthermore, Figure 4(b&c) shows the stacked spectrum of all load steps. The resonances, indicated by darker orange lines, are seen to shift in value and to follow the load increase and subsequent decrease. It demonstrates that resonances exhibit different sensitivities to the applied compressive load. However, it is expected that the applied compressive load will result in a lower resonance frequency (softening instead of stiffening) *(2)*. A similar phenomenon, also showing stiffening with compressive load, can be found in *(3)*.

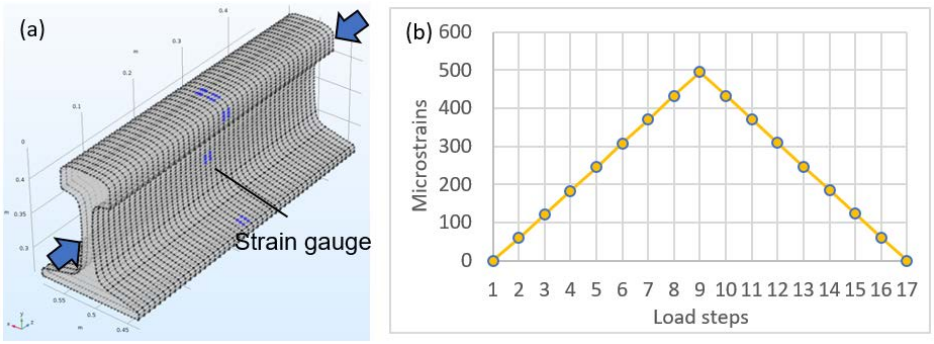

Figure 3: (a) Compression test configuration; (b) applied strain history

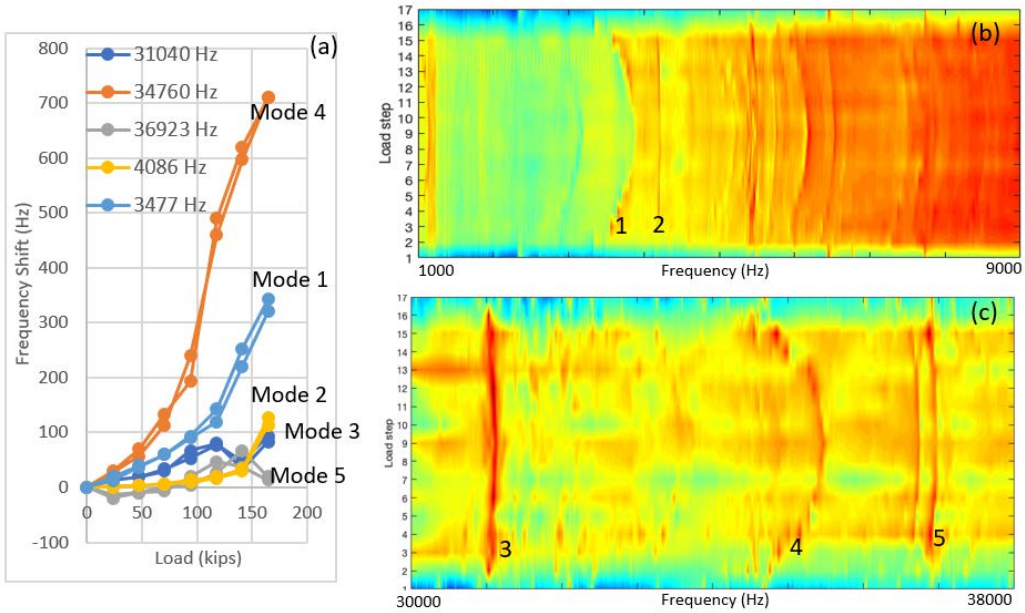

Figure 4: For a rail subjected to compressive loading, (a) frequency shifts of selected resonances during loading; stacked spectra for the entire load history (b) from 1 kHz-9 kHz and (c) from 30-38 kHz

To investigate the temperature effect, a test was conducted on the same piece of 132RE rail. The rail sat on a dolly with supports at its ends, and it was assumed to expand freely with temperature variations. The specimen was then exposed to strong sunshine for eight

hours and monitored the temperature change. Figure 5(a) shows the test setup, and the rail temperature changed over the day, as shown in Figure 5(b). Downward shifts in resonance frequencies (softening) with increasing temperature are clearly obersved, as shown in the stacked spectrum of Figure 5(c). Track resonances demonstrate a frequency-dependent behavior under temperature variation.

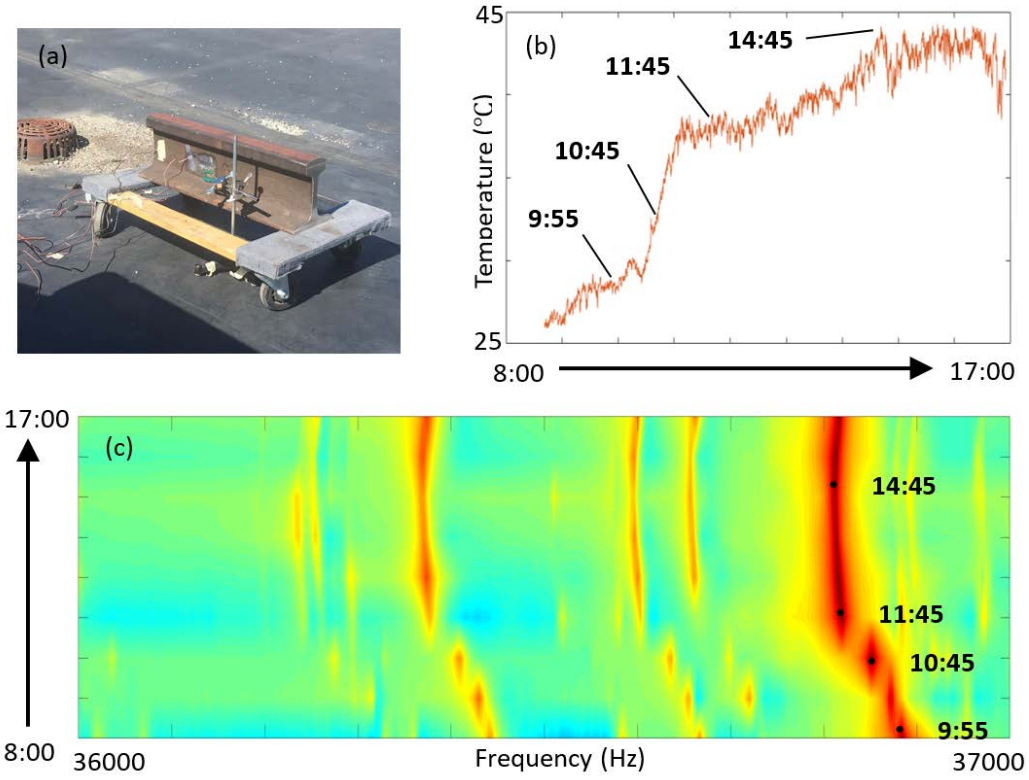

Figure 5: (a) temperature test configuration; (b) recorded rail temperature throughout the day; (c) stacked spectrum for the entire temperature history

Task 3: Select an in-service CWR track section test site for field tests and instrument the rail with continuous strain and temperature data logging system

The team worked with the railway partner, BNSF, to identify an appropriate in-service CWR site on an active rail line in Illinois. A suitable test location for the field tests was identified: Milepost 87 on the Chillicothe subdivision on the Main 2 line near Streator, Illinois. Figure 6 shows the location of the test site, which is about a 2-hour drive from Champaign-Urbana. During field data collection, BNSF provided access to the field site and ensures track security for all participants.

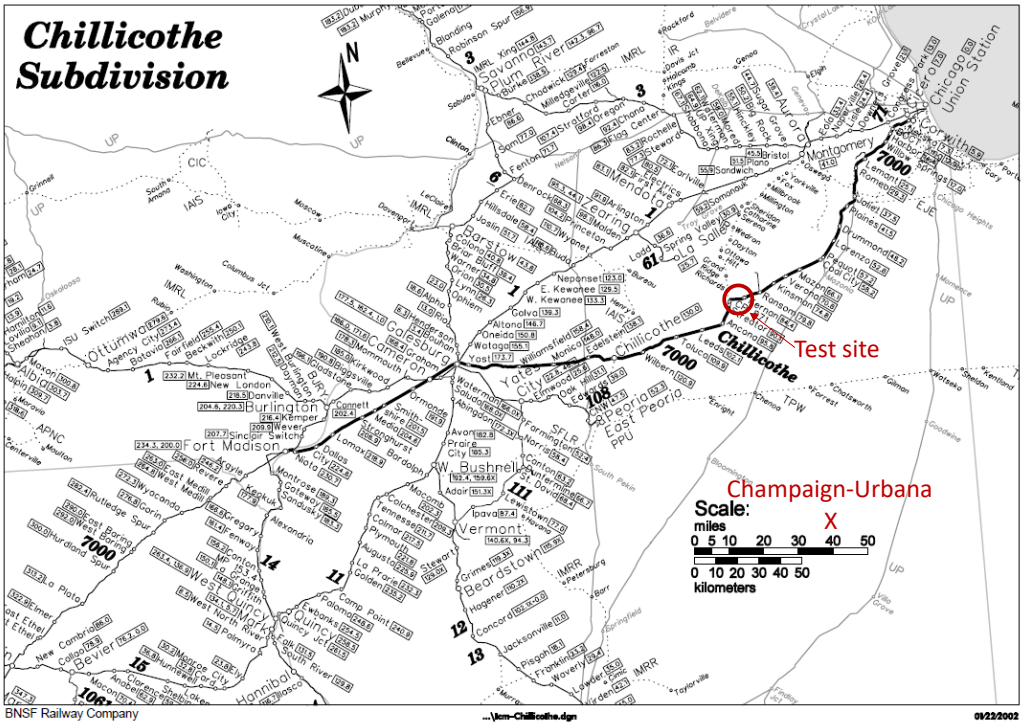

Figure 6: Map showing location of rail test site, located on BNSF Chillicothe subdivision line

Task 4: Coordinate de-stressing procedure with railroad partner and calibrate long-term strain to absolute values

Coordinating with BNSF, a de-stressing procedure was performed on fully instrumented rail sections at the selected Streator test site, while the installed full-bridge strain gauges were calibrated for zero strain to ensure an accurate RNT measurement.

On July 29, 2019, a contractor, Instrumentation Service, Inc. (ISI), installed strain and temperature sensors on one rail at the selected test site. As shown in Figure 7, strain gauges and RTD temperature sensors were mounted directly on the rail web close to the rail neutral axis at two locations about 5 yards (15 feet) apart. The third set of gauges that detect passing trains was also installed. The sensors are connected to a solar-powered data logging system that regularly collects and sends data to a cloud storage site. All data are accessible by the research team through a web-based interface. The sensing system was checked and confirmed to be fully operational on the evening of July 29, 2019.

A BNSF maintenance crew carried out a rail de-stressing procedure on the instrumented rail on the morning of July 30, 2019, as shown in Figure 8. And the strain gauges were zeroed by applying an offset to the measured voltage output of the Wheatstone bridge circuit, where the offset value is set as averaged circuit output voltage between rail cutting and welding. The automated system reports rail temperature, axial strain, axial load, and RNT at a 15-minute interval and uploads the data to a website, whose user interface is shown in Figure 9.

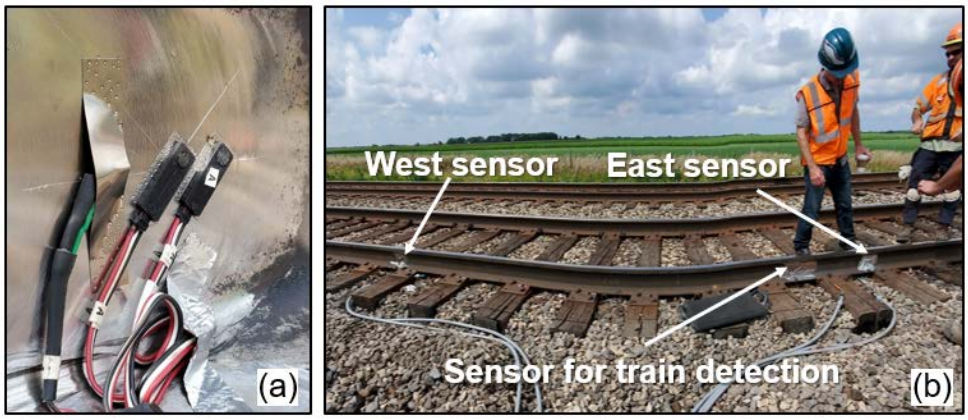

Figure 7: Detail of rail instrumentation: (a) individual strain and temperature gauges mounted at one location, and (b) two sensor set locations after mounting completion

Figure 8: Detail of rail destressing process: (a) rail cut located between position of two sets of gauges, and (b) completed weld after the cut

ISIRAIL.COM Monitors Data uuiuc

Quick search

(Site = RNT Streator IL UUIUC) And (Mile Post = 86.999)

Site	Timestamp	Mile Post	Rail ID	Neutral Temp	Rail Temp	Rail Force	SG Voltage	SG Offset	Trackid
RNT Streator IL UUIUC	2019-08-31 08:10:03	86.999	S	83.6	69.1	-34426	0.65	1.07	
RNT Streator IL UUIUC	2019-08-31 08:05:03	86.999	S	83.3	68.5	-35227	0.65	1.07	
RNT Streator IL UUIUC	2019-08-31 08:00:04	86.999	S	83.2	67.7	-36829	0.63	1.07	
RNT Streator IL UUIUC	2019-08-31 07:55:02	86.999	S	83.0	66.3	-39633	0.59	1.07	
RNT Streator IL UUIUC	2019-08-31 07:50:02	86.999	S	82.8	65.1	-42036	0.56	1.07	
RNT Streator IL UUIUC	2019-08-31 07:45:04	86.999	S	82.7	64.4	-43638	0.54	1.07	

Figure 9: Screenshot of the cloud storage website that shows RNT, rail temperature, rail force, and strain records

Data obtained from the instrumented rail sections demonstrated reasonable and expected results, suggesting that the stress-relieved rail structure and data collection system have been operating properly. Figure 10 shows the measured rail strain during the time before and after the rail stress relief procedure. The data shows that the rail cut effectively relieved the longitudinal residual stress that had existed in the rail, allowing us to identify the zero-stress state in the rail based on the strain output. Typical temperature and strain variations of the instrumented rail well after the rail de-stressing operation are shown in Figure 11, where a clear connection between increasing rail temperature and increasing axial compressive strain can be identified. The relationship between strain and rail temperature over one month of data logging is shown in Figure 12. Each day of data collection is represented by different colored points. The average slope of a line fit to the data is 6.57 microstrain per degree Fahrenheit, which is close to the nominal thermal expansion coefficient of rail steel (6.5 με/°F). The general trends of rail temperature and strain over the long term from August 1st to October 31st, 2019, are shown in Figure 13. The rail temperature and strain demonstrate expected variations with seasonal changes.

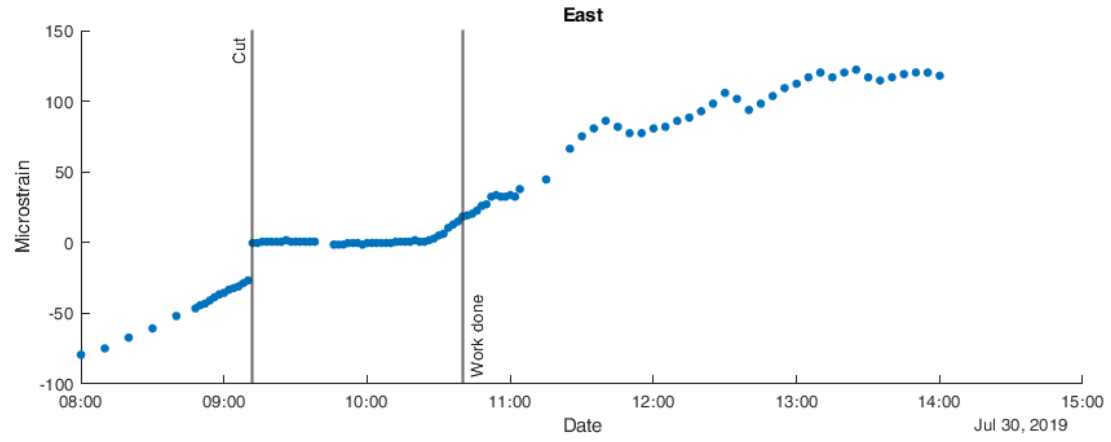

(a)

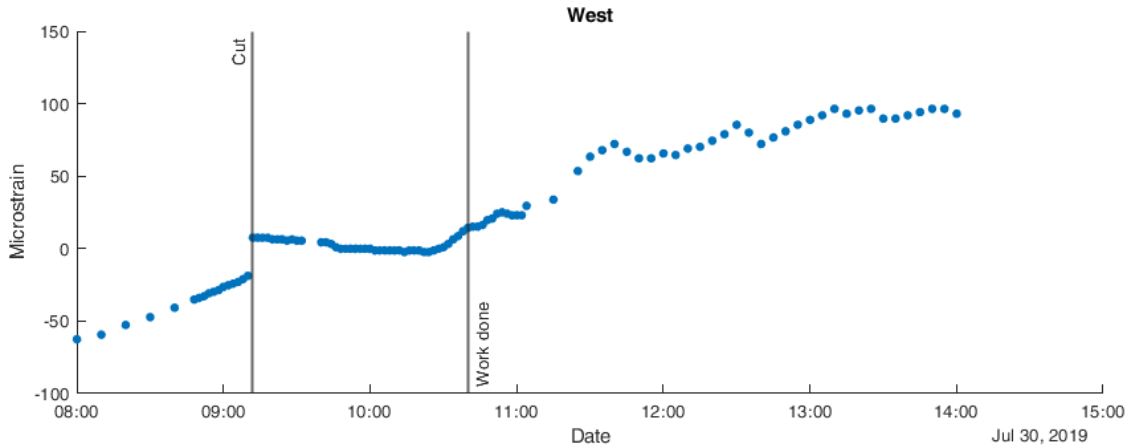

(b)

Figure 10: Strain output from the instrumented rail from east (a) and west (b) test locations on July 30, 2019. Occurrence time of rail cut and rail weld associated with the rail de-stressing procedure are indicated

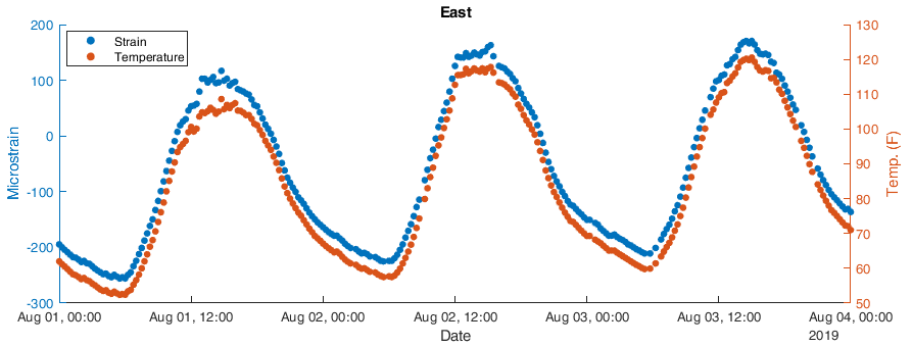

(a)

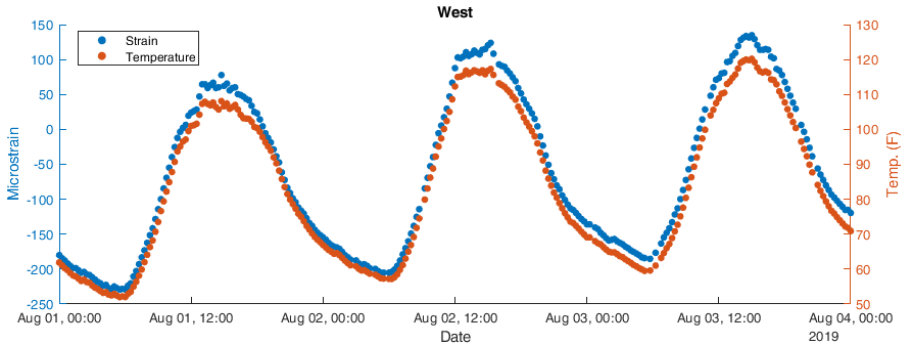

(b)

Figure 11: Rail temperature and axial strain as a function of time over several days. Data collected from east (a) and west (b) test locations between Aug. 1 and Aug. 3, 2019

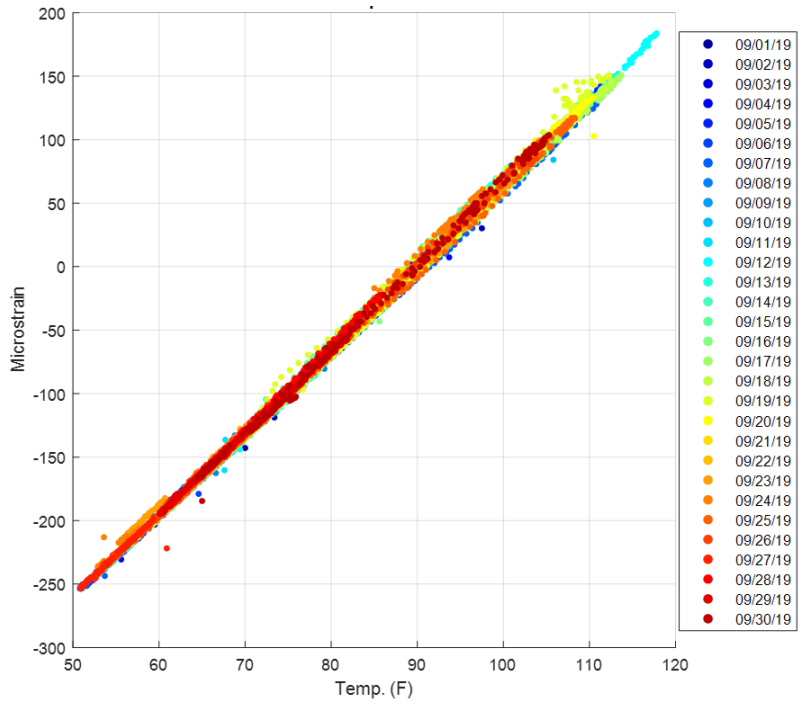

Figure 12: Axial strain as a function of rail temperature. Data collected from east test location between Sep. 1 and Sep. 30, 2019

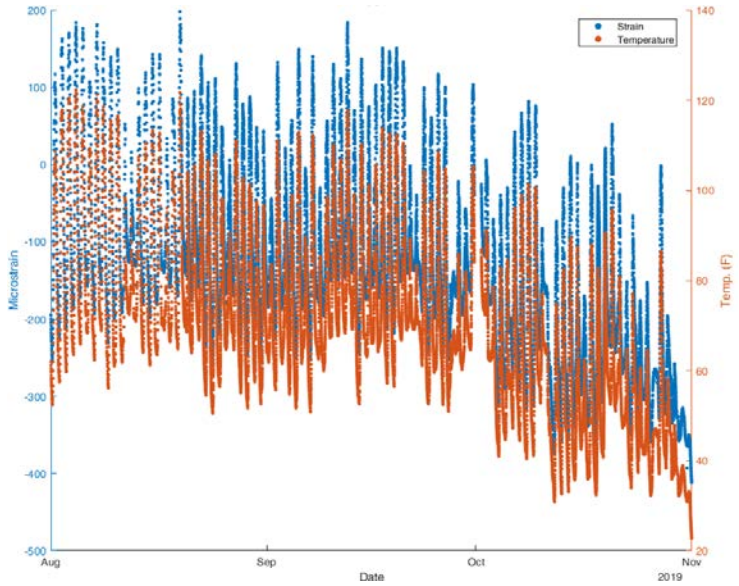

Figure 13: Rail temperature and axial strain as a function of time over several months. Data collected from the east test location between Aug. 1 and October 31, 2019

Figure 14 shows the rail temperature and RNT on the east test location. The RNT was calculated using the measured temperature and strain, and it shows a relatively consistent behavior over the short term regardless of the rail temperature changes. The long-term behavior of RNT is shown in Figure 15. Rather than showing all rail temperature data, daily average rail temperature was plotted in the figure for simplicity. Generally, with the decreased daily average rail temperature, the RNT shifts approximately from 92.5°F to 80°F over 4 months after de-stressing. According to the team's internal communication with Mr. A. Kish and Mr. H. Harrison, the slowly decreasing RNT is expected, especially after the cut as the system tries to reach its lowest energy state. A sudden drop in RNT was observed in November. These can be caused by temperature drop due to seasonal changes.

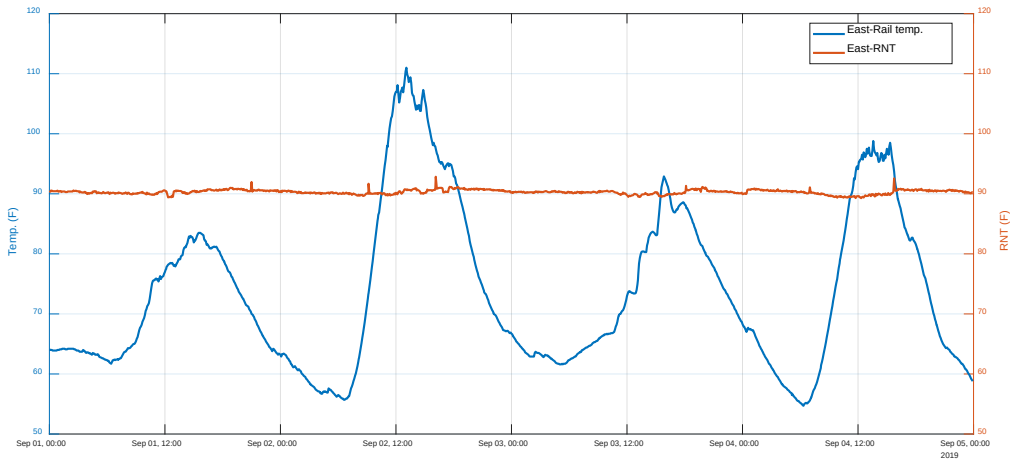

Figure 14: Rail temperature (blue line) and RNT (orange line) as a function of time over several days. Data collected from east test locations between Sep. 1 and Sep. 4, 2019

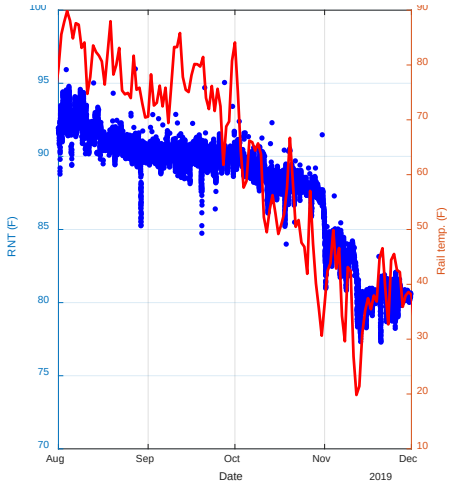

Figure 15: RNT (blue dots) and rail temperature (red line) as a function of time. Data collected from east test location between Aug. 1 and Nov. 30, 2019

Task 5: Collect vibration data from instrumented test site

The goal of this task was to collect a large volume of rail vibration data across different stress conditions that can be correlated to temperature and RNT values of rail at the selected site location, and thus serve as input to machine learning algorithms.

After the rail destressing procedure was completed on July 31, 2019, the team started vibrational data collection. Each set of vibration data collection involves a day-long visit to the instrumented track test site. Vibration data are collected from the "east" and "west" test locations approximately every 30 minutes throughout the day as the rail temperature varies naturally. For each vibration data collection event, the microphone holding arm was positioned next to the track, and the microphone was placed into one of the five possible monitoring positions, as shown in Figure 16(a). Then the metallic impactor was manually applied (by hand) on the surface of the rail at another one of the five testing positions; see Figure 16(b). For each impactor-sensor configuration, ten impact events were applied, and the vibration data measured. Keeping that same microphone position, the impact point was moved to the next position around the rail cross-section, and data were collected. When all impact positions were completed, the microphone was moved to the next sensing position, and the process was repeated to obtain data from all possible impactor-sensor configurations.

A summary of the six field data collection events to date is provided in Table 1. Over the six field visits, more than 40,000 vibration signals were collected. It is notable that the rail temperature ranges are similar at east and west sites, but the strain ranges are not. A difference of 10 to 40 microstrain between east and west sites is observed. The team investigated possible causes for this discrepancy and has excluded the possibility of a malfunctioning amplifier at the west test site. For each test location and rail temperature condition, at least ten vibrational responses for each testing position combination of A through E around the rail profile are collected. Thus, a large volume of test data was obtained.

(a) (b)

Figure 16: Data collection configuration using metallic impactor and contactless acoustic sensor: (a) microphone holding arm placed next to the rail and sensor positioned at location "A" and (b) applying the metallic impactor on the rail to generate vibration signals.

Table 1: Details of field test visits in 2019

Test date	Rail Temperature range (°F)		Rail strain range (Microstrain)		Total number of vibration data collected
	West	East	West	East	
August 1	64 ~ 108	64 ~ 109	-162 ~ 78	-175 ~ 117	~6870
August 5	75 ~ 119	75 ~ 119	-93 ~ 152	-110 ~ 172	~8940
August 15	67 ~ 113	67 ~ 113	-120 ~ 128	-154 ~ 142	~6220
August 29	60 ~ 103	60 ~ 101	-150 ~ 88	-196 ~ 87	~7700
September 19	61 ~ 113	61 ~ 112	-142 ~ 144	-189 ~ 151	~4780
October 18	37 ~ 83	37 ~ 83	-252 ~ 3	-330 ~ -29	~5810

The vibration test data demonstrate good quality with minimal ambient disruption and a reasonably high signal-to-noise ratio. Figure 17 shows a typical vibration spectrum collected from the instrumented rail using two different test configurations. The spectra show clear resonant peaks that are associated with cross-sectional resonance responses of the rail. Note that the responses vary by the test configuration. For example, for test configuration C-C, resonances at 37 and 39 and 76 kHz can be identified, while we see resonances at 31 and 41 kHz with configuration E-E. For all test configurations, we obtain vibrational responses across a broad range of frequencies with our data collection system, providing a rich data set for further analysis.

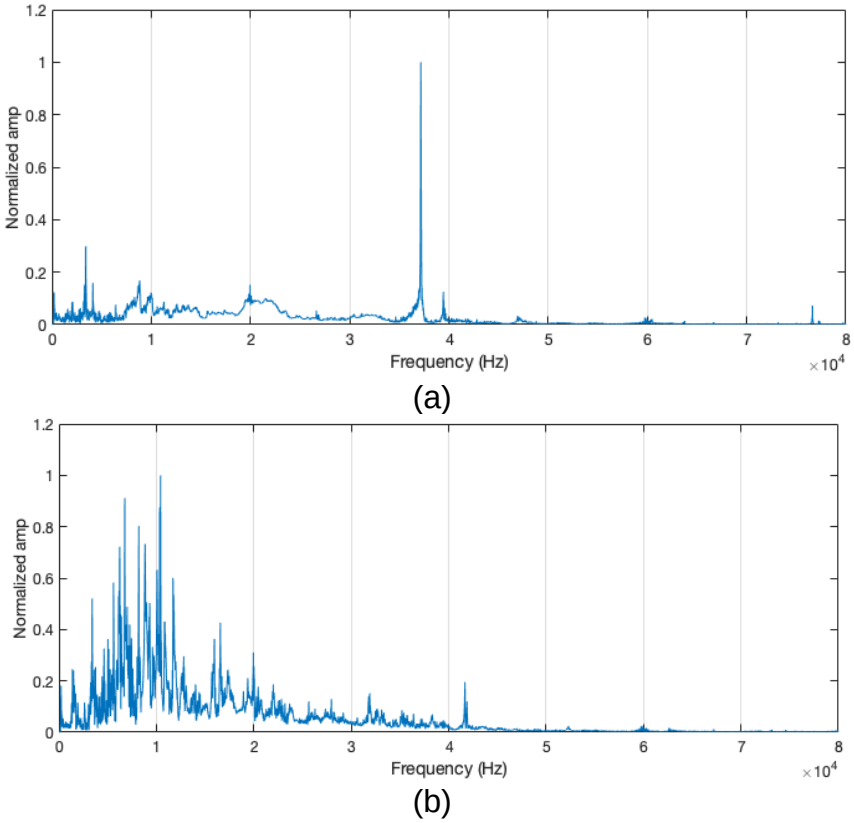

Figure 17: Typical resonance spectra obtained from the east test location on Aug. 5 using the C-C (a) and E-E (b) test configurations

The vibration spectral data show a clear sensitivity to the changing thermal stress. Figure 18 demonstrates a stacked plot of spectra collected from a single day of testing from one test location. The plot shows a clear variation of resonance frequencies with rail stress conditions: as rail temperature and rail compressive stress increase, the resonance frequencies decrease, but at different rates from each resonance. After the maximum temperature (and strain) of the day were reached, the frequencies of those sensitive resonances start to increase. The dependency of resonance frequency on temperature and strain is clearly illustrated in Figure 19, where the frequency appears to be linearly associated with the change of the temperature and axial stress in the rail.

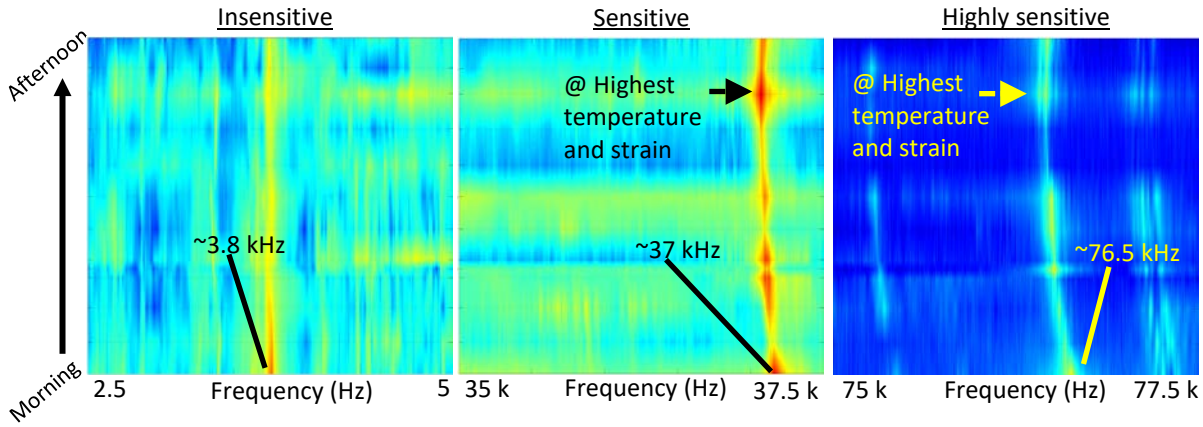

Figure 18: Stacked spectral plots of resonances showing different sensitivities to the rail temperature and stress change throughout a day of testing. Data collected on Aug. 5, 2019 at the east test site

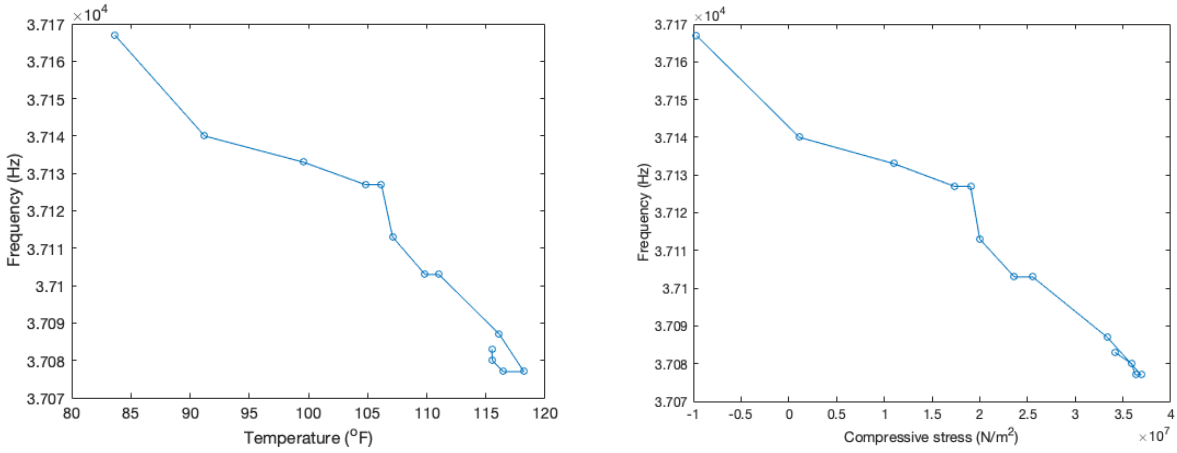

(a) (b)

Figure 19: Change in resonance frequency of the 37 kHz mode as a function of (a) rail temperature and (b) axial rail stress throughout a day or testing. Data collected on Aug. 5, 2019 at the east test site

Stage 2: Machine learning for RNT determination based on field data

Task 6: Formulate and evaluate neural network architecture

In this task, the team formulated a machine learning framework for RNT prediction by (i) exploiting finite element analysis to interpret field data and understand the behavior of vibrational modes under thermal loads; (ii) designing a regression model that reflects how modal frequencies vary with thermal stress; (iii) establishing a neural network to correlate modal frequencies with RNT.

Task 6.1: Finite element analysis for cross-sectional modes

A time-dependent finite element model is designed to interpret the field data. We obtained the time-domain response of a simulated segment of rail track subjected to an impact event. To best approximate the rail geometry, the rail cross-section is obtained by scanning the cut rail piece from the rail destressing location at the field site; see Figure 20. Rail cross-section information can be obtained from a rail profile measuring system. The simulated rail segment is simply supported at the bottom, and a low reflective layer boundary is applied at both ends of the rail to simulate a track with an infinite length. An impulse boundary load is applied at the midspan of a short piece of rail. With an impact location at the center of rail head (A), the structural response at the side of rail head (C) is recorded and analyzed using FFT to understand its spectrum pattern; see Figure 21(b). Vibrational response collected along the center of rail head are recorded and processed with 2D FFT to illustrate its dispersion behavior; see Figure 21(c). Comparing Figure 21(a) - the experimentally obtained data from field observations using the A-C configuration with Figure 21(b) - the simulated spectrum, we see a good match in frequencies for the resonance modes at 31 and 37 kHz. These modes align with zero-slope points in the frequency-wavenumber domain ($\partial\omega/\partial k = 0$) shown in Figure 21(c), marked with red dotted lines, which further confirms that the designed experimental setup promotes the excitation of zero-group velocity (ZGV) modes. The ZGV modes are known to support high signal-to-noise ratio measurement and insensitivity to boundary condition variations *(4)*.

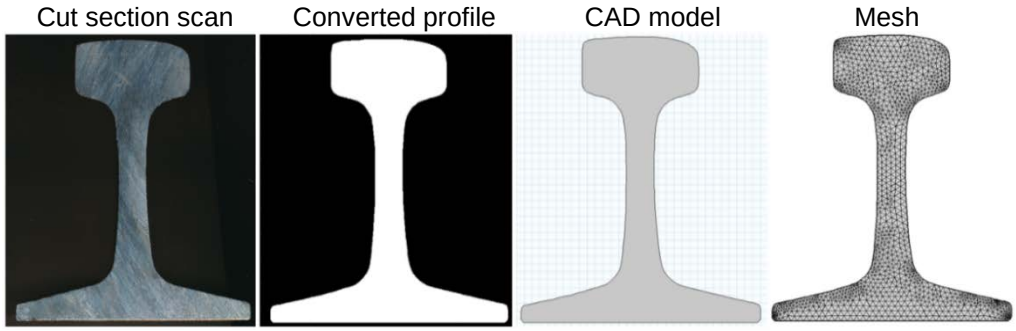

Figure 20: Conversion of rail cross-section obtained from cut rail section to FE model mesh geometry

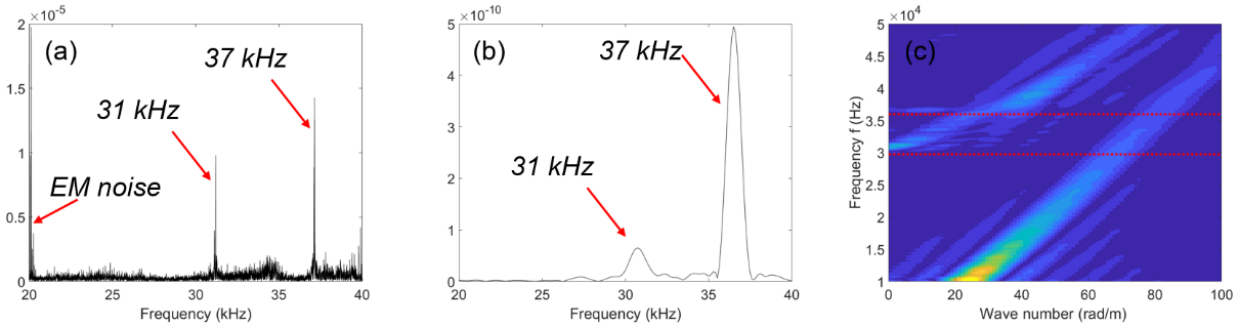

Figure 21: (a) Spectral field data using A-C configuration; (b) Spectral FEM data using A-C configuration; and (c) dispersion curves generated by FEM data on the same rail cross-section

Considering the fact that ZGV modes are predominant in the field data collected at Stage I, the team designed another finite element model to understand behaviors of cross-sectional vibrational modes when the confined rail is subjected to thermal load. As shown in Figure 22, a two-step analysis is conducted on a simulated segment of rail. In step 1, a prescribed displacement (displacement along z-direction w=0) is imposed so that the nodes at both ends of the rail are confined at z-direction, where a fixed constraint and roller support condition is configured at the rail foot to avoid rigid body solutions. The rail temperature is imposed on the entire sample to simulate the thermal expansion of the rail. In step 2, only the prescribed displacement is imposed at both ends, and an eigenfrequency analysis is conducted. This modeling procedure is designed to simulate eigenfrequencies of continuous axially confined rail based on its updated global stiffness matrix *(5)* caused by thermal expansion. While flexural, torsional, and coupled modes also present, this study focuses on cross-sectional modes because (i) the designed experimental setup promotes cross-sectional modes in CWR; (ii) cross-sectional modes are insensitive to boundary conditions, such as tie condition and spacing, fastener and clip condition, etc.; and (iii) cross-sectional modes are not length-dependent, which further simplifies modeling efforts.

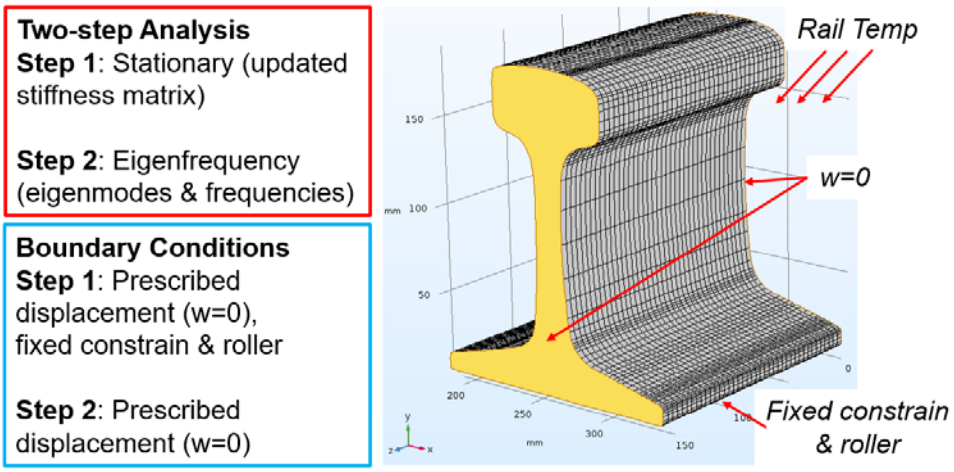

Figure 22: Finite element model simulating cross-sectional vibrational modes' behavior

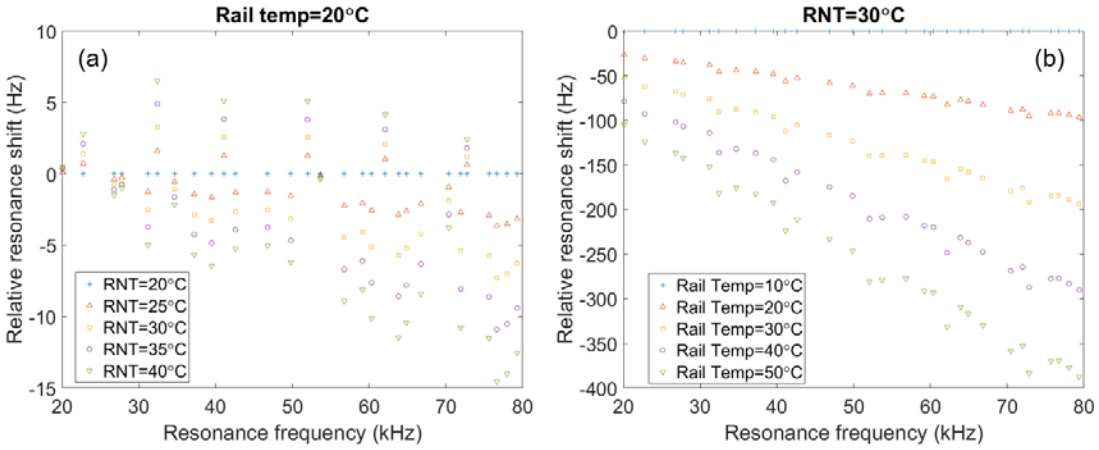

Figure 23: Illustration of how cross-sectional modal frequencies vary because of (a) changing RNT at fixed rail temeprature and (b) changing rail temperature at fixed RNT

To understand the influence of mechanical and thermal loads on ZGV modes, the team performed a series of FE simulations of ZGV modes of a confined segment of rail with rail temperature ranging from 5 to 50ºC and RNT ranging from 20 to 40ºC, which well cover the rail temperature and RNT data obtained in the field data. A parametric representation of those data is shown in Figure 23. Figure 23(a) shows the relative resonance shift of selected resonance frequencies is plotted against the original modal frequency for varying RNTs (axial load levels) at a fixed rail temperature of 20ºC. A 20ºC difference in RNT can lead to a 50 MPa difference in thermal stress for AREMA 136RE rail. The 136RE cross-section was selected because that represents the rail in our field test site. Within the frequency range of 20 to 80 kHz, cross-sectional modes shift towards lower frequency as the rail is subjected to increasing tensile load (higher RNT) at constant rail temperature. And the modes shifting towards higher frequency are the flexural and torsional ones, which is not of interest. Figure 23(a) demonstrates the modest extent of variation in cross-sectional modal frequencies introduced by RNT or mechanical axial load, independent of temperature. Figure 23(b) shows larger extents of variation in cross-sectional modal frequencies caused by the temperature at a constant RNT. Within the frequency range of 20 to 80 kHz, cross-sectional modes shift towards lower frequency with an increasing rail temperature. It is notable that Figure 23(b) demonstrates a level of variation in cross-sectional modal frequencies introduced by both rail temperature and axial load. Both observations confirm expectations and provide a solid foundation for the proposed regression model.

Task 6.2: Regression model for cross-sectional modes under thermal loads

In light of the fact that cross-sectional modal behavior under mechanical and thermal loads, a regression model is well-suited to correlate modal parameters (input) with RNT (output). A simple mathematical formulation is presented to relate multi-modal rail vibration features $\vec{f}$ to ΔT - the difference between rail temperature and RNT.

$$\vec{f} = \vec{f}_{RNT} + \boldsymbol{S}_{\sigma T}\overrightarrow{\Delta T} \tag{1}$$

where the feature vector $\vec{f}$ is composed of the measured multiple vibration features $(f_1, f_2 \dots, f_{n-1}, f_n)$, the vector $\vec{f}_{RNT}$ represents the same feature vector when the measurements are conducted at RNT conditions, and $\overrightarrow{\Delta T}$ contains the information of RNT, rail temperature, and thermal stress. The $\vec{f}$ and $\overrightarrow{\Delta T}$ data are related through the $\boldsymbol{S}_{\sigma T}$ matrix, which describes axial load and temperature sensitivities corresponding to each of the features in $\vec{f}$. The equation above is more clearly illustrated in matrix form

$$\begin{Bmatrix} f_1 \\ f_2 \\ \vdots \\ f_{n-1} \\ f_n \end{Bmatrix} = \begin{Bmatrix} f_1^{RNT} \\ f_2^{RNT} \\ \vdots \\ f_{n-1}^{RNT} \\ f_n^{RNT} \end{Bmatrix} + \begin{bmatrix} S_1^{\sigma} & S_1^{T} \\ S_2^{\sigma} & S_2^{T} \\ \vdots & \vdots \\ S_{n-1}^{\sigma} & S_{n-1}^{T} \\ S_n^{\sigma} & S_n^{T} \end{bmatrix} \begin{Bmatrix} -E\alpha\Delta T \\ \Delta T \end{Bmatrix} \tag{2}$$

where we see that S_k^{σ} stands for the temperature-induced stress sensitivity of the kth feature f_k of the data set and S_k^{T} stands for the temperature sensitivity of f_k. The

developed thermal stress is estimated as $-E\alpha\Delta T$, where E is the elastic modulus of rail, and α is the coefficient of thermal expansion of rail steel. This all represents a simple linear expression in the form of "y = mx+b" where independent (ΔT) and dependent (f_k) known variables are related to each other through unknown coefficients ($\boldsymbol{S}_{\sigma T}$ and f_k^{RNT}) that need to be determined through a regression analysis. Once a regression analysis is carried out to "best fit" the known variables through the determined coefficient values, this relation can be used to predict RNT with signal features ($\vec{f}$), and vice versa. It is notable that rail temperature is necessary for RNT determination during this process and can be obtained in a field environment.

Task 6.3: Neural networks for RNT prediction

While it is possible to conduct a generalized linear regression model to estimate the coefficients, advancement in neural network opens new avenues that can massively outperform traditional methods for regression. Instead of computing regression coefficients, neural networks are "trained" using sets of known parameters until it reaches a form that sufficiently works to predict RNT from a set of signal parameters. Machine learning approaches have been successfully applied to address issues in transportation engineering, including problems that are similar to the one we address in this study *(6)*. Machine learning is analogous to regression, wherein the simplest case known data sets are related to each other through an equation.

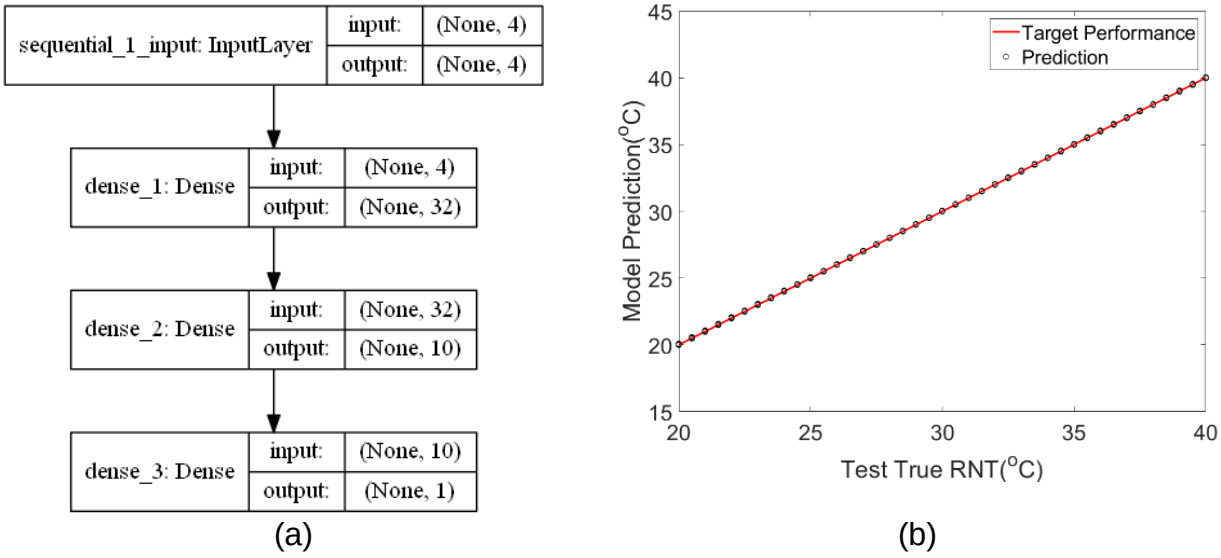

Figure 24: (a) Neural network for RNT prediction; (b) RNT prediction results using FEM data

The team designed the structure of a machine learning framework that exploits a neural network for RNT prediction. The input vector $\vec{f}$ includes resonance frequencies of cross-sectional modes and rail temperature, and the output layer is a scaler for RNT prediction. A fully-connected neural network architecture is composed of two hidden layers, followed by an output layer, as shown in Figure 24(a). The NN is optimized using a large set of well-calibrated synthetic data produced with our own FEM using the Comsol 5.4 platform. The input dataset is divided into training, validation, and testing subsets.

The majority of the dataset will be used for the purpose of network training: 70% of the entire data set will be randomly selected. Then the trained network will be verified with a validation dataset comprising 15% of the data remaining in the pool that is randomly selected to prevent over-fitting. The amount of training data is determined based on the Vapnik-Chervonenkis dimension *(7)*. Finally, the NN performance for predicting RNT from input data will be evaluated with the remaining 15% of the data pool. The architecture has been implemented using Python 3.7 and TensorFlow 1.14.0 platform. As shown in Figure 24(b), RNT predictions resulted from resonance frequencies of 31, 37, and 39 kHz are perfectly aligned with the target performance, which confirms the feasibility of using NN and cross-sectional modes for RNT prediction. The group of resonances is chosen since they are the most predominant ones in field data collection.

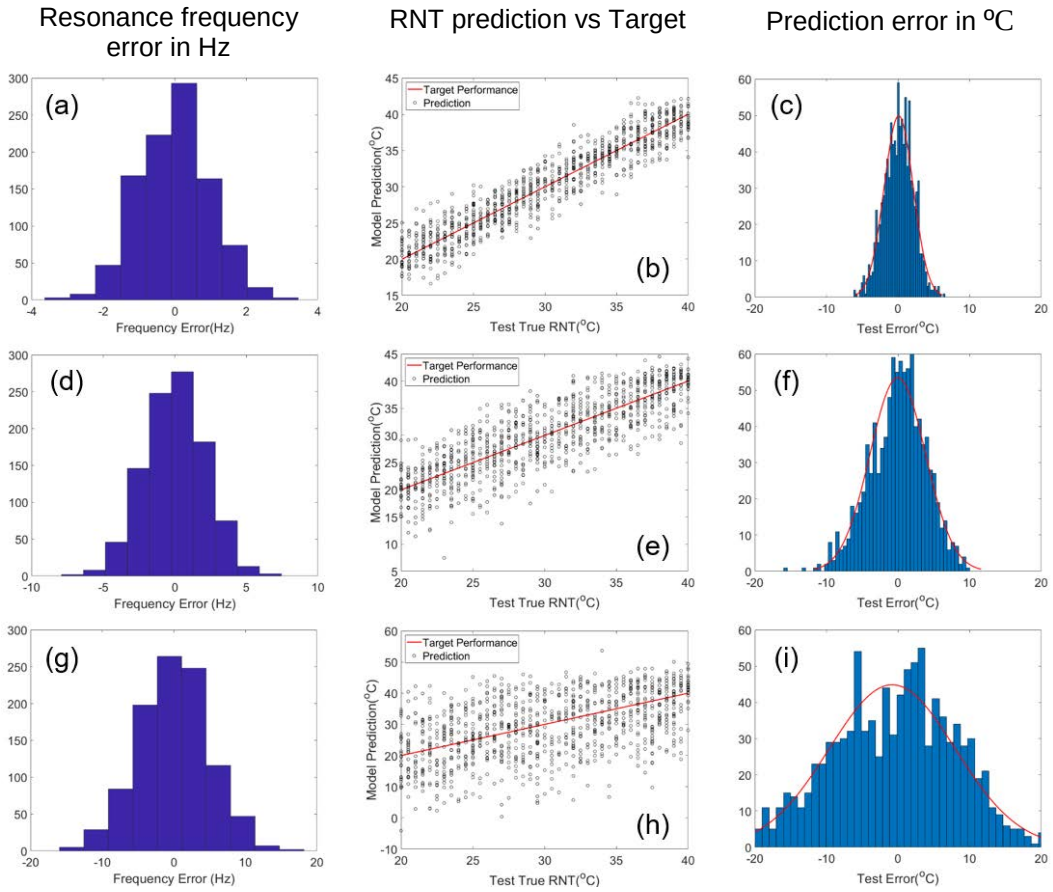

Figure 25: Effect of signal noise level on RNT prediction for 31, 37, & 39 kHz mode data: noise levels 1 (a-c), 2 (d-f), and 5 (g-i)

To better understand the influences of signal noise and uncertainty on system performance, the resonance frequencies of selected modes of vibration containing different levels of artificial random noise are used as inputs to the neural network. The prediction results are shown in Figure 25. Signal noise is introduced by adding normally distributed random noise to FEM simulated resonance data with standard deviations of

1 (level 1), 2 (level 2), and 5 (level 5), respectively. For data using resonances of 31, 37, and 39 kHz, noise level 1 can support RNT prediction with an accuracy of ±2ºC (±3.6ºF) with a 68% confidence interval (CI) or ±4ºC (±7.2ºF) with a 95% CI; noise level 2 can support RNT prediction with an accuracy of ±3.8ºC (±6.84ºF) with a 68% CI or ±7.8ºC (±13.68ºF) with a 95% CI; noise level 5 can support RNT prediction with an accuracy of ±8.6ºC (±15.5ºF) with a 68% CI or ±17.2ºC (±31ºF) with a 95% CI. These results suggest that measurement/model with noise level 1 can provide satisfactory RNT prediction performance when using resonance modes at 31, 37, and 39 kHz.

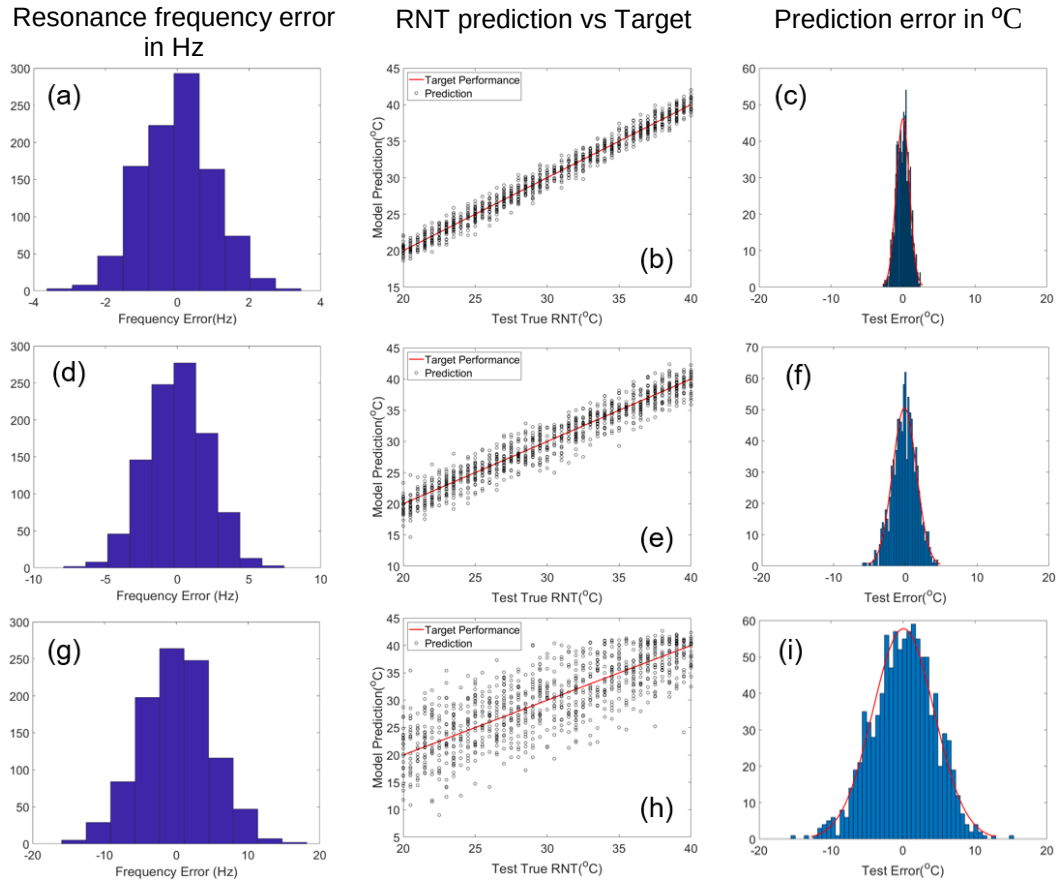

Figure 26: Effect of signal noise level on RNT prediction for 76, 78, & 79 kHz mode data: Noise levels 1 (a-c), 2 (d-f), and 5 (g-i)

It is notable that 31, 37, and 39 kHz resonances were selected as a result of the experimental setup, which can be optimized in future research. The NN with the same architecture is trained with FEM data using resonances of 76, 78, and 79 kHz. A significant improvement in terms of RNT prediction can be achieved with the selected resonance group, as shown in Figure 26. Noise level 1 can support RNT prediction with an accuracy of ±0.9ºC (±1.6ºF) with a 68% CI or ±1.8ºC (±3.24ºF) with a 95% CI; noise level 2 can support RNT prediction with an accuracy of ±1.7ºC (±3ºF) with a 68% CI or ±3.4ºC (±6ºF) with a 95% CI; noise level 5 can support RNT prediction with an accuracy of ±4.2ºC (±7.6ºF) with a 68% CI or ±8.4ºC (±15ºF) with a 95% CI. It concludes that measurement/model with noise/error up to level 2 can provide satisfactory RNT prediction performance when using resonances of 76, 78, and 79 kHz.

Task 7: Optimize input feature selection and NN architecture by evaluating system performance using field data that contain broad variations in rail temperature

In this task, model parameters are first calibrated based on field data, including Young's modulus (E), Poisson's ratio (ν), the density of rail steel (ρ), and the temperature sensitivity of Young's modulus. The temperature sensitivity of Young's modulus is estimated by comparing COMSOL model prediction with an experimental study on a free-to-expand rail under temperature variations. The temperature sensitivity of -0.054 GPa/ºC is identified with the closest estimation, and is similar to the nominal property.

To get parameter estimation on E, ν, and ρ, a series of models are simulated with field observations on rail temperature and RNT. For each field observation, we swept ν from 0.274 to 0.280 with a step size of 0.002, ρ from 7640 to 7800 kg/m^3 with a step size of 20, and E from 207 to 213 GPa with a step size of 0.5 GPa. Interestingly, with constant rail temperature and RNT, a linear correlation can be identified between model parameters and resonance frequency. Therefore, a multivariable linear regression model is established to represent the relationship among resonance frequencies and E, ν, and ρ

$$\theta_1 E + \theta_2 \nu + \theta_3 \rho + \mathrm{b} = \mathrm{f} \tag{3}$$

where θ_1, θ_2 and θ_3 are coefficients of E, ν, and ρ, b is the bias term, and f is a resonance frequency. And a matrix representation can be written as

$$A * X = \mathrm{f} \tag{4}$$

where $A = [\theta_1, \theta_2, \theta_3, 1]$ and $X = [\mathrm{E}, \nu, \rho, b]^T$. Furthermore, this relationship can be extended for multiple resonance frequencies, and A can be determined for each resonance at fixed rail temperature and RNT. By comparing model predictions ($A * X$) with all the field vibrational data (y), parameters in matrix X can be determined. It is formulated as a convex optimization problem to find desirable parameters of E, ν, and ρ, by searching for solution of

$$\min\{(A * X - y)^2\} \tag{5}$$

with constraints of 207×10^9 < E < 213×10^9, 0.270 < ν <0.280, and 7640 < ρ < 7800. The problem is solved with CVX ver. 2.2. It is notable that similar information can be obtained by performing ultrasound velocity measurements close to working frequency in the field.

Second, the team updates the NN architecture (developed in Task 6) with calibrated FE models and now evaluates its performance using the dataset obtained from the field test site (Task 5 of Stage I). Resonance frequencies of resonance modes at 31, 37, and 39 kHz, along with rail temperature, are used as inputs to the trained NN. First, a mismatch ranging from -40 to 30 Hz between field measurements and model prediction can be observed, as shown in Figure 27(a). The mismatch can result from two issues: (i) 31 and 39 kHz resonances are not always effectively promoted in field data collection and sometimes can be buried within the noise floor; this also applies to other resonance modes including 28, 41, 61, and 76 kHz; and (ii) uncertainty of model parameters for the FE models. While the error in resonance frequency prediction is lower than 0.1%, the experimental noise level is higher than that represented by noise level 5 shown in Figure

25(g), and thereby lead to unsatisfactory performance in terms of RNT prediction, as illustrated in Figure 27(b&c).

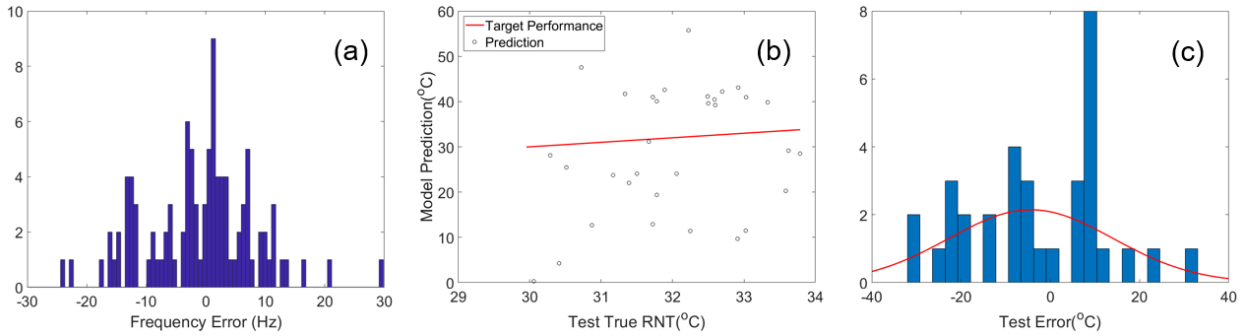

Figure 27: Field data with resonances of 31, 37, &39 kHz modes (a) model prediction error on resonance frequencies in Hz, (b) RNT prediction, (c) RNT prediction errors in °C

The team also investigated the performance of using individual resonance peak frequency and rail temperature as inputs, and trained three neural networks using the resonance data of 31, 37, and 39 kHz, respectively. The NNs are designed with the same architecture as Figure 24(a), except for the dimension of the input layer. A selected group of measurements based on resonance frequency mismatch are shown in Figure 28, where individual resonances are used for RNT prediction. As expected, measurements of minimum discrepancies with regard to numerical models can support RNT prediction with reasonable accuracy of ±5.5°C (±9.9°F), as shown in Figure 28(c).

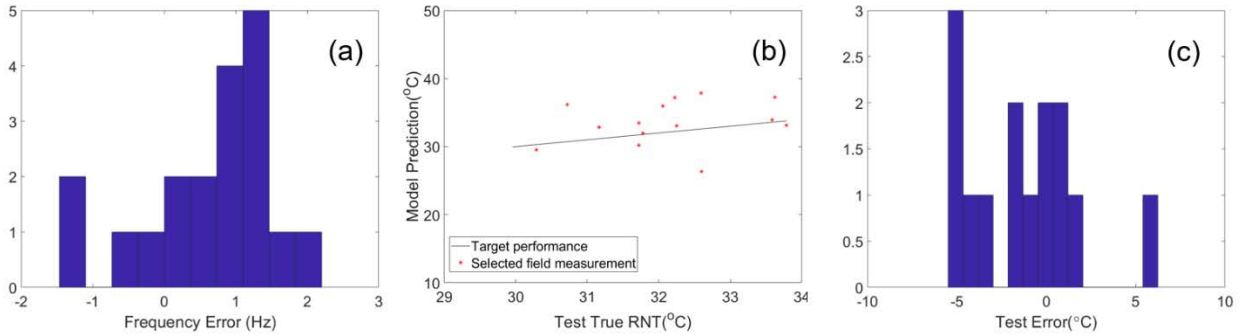

Figure 28: Selected field data using individual resonances (a) model error in Hz, (b) RNT prediction, and (c) RNT prediction errors in °C

Task 8: Extend NN results to other structural cases using synthetic data produced by finite element simulation

To evaluate the versatility of the developed framework to other rail structure cases beyond the one considered in the field site, which is AREMA 136RE with some rail wear, the team carried out analysis using vibration data created with FEM on a standard AREMA 132RE cross-section in COMSOL 5.4. A 3-D FEM was created to simulate the

behavior of cross-sectional modes under thermal loads of rail temperature ranging from 5 to 50°C, and RNT ranging from 20 to 40°C, which well cover the rail temperature and RNT data obtained in the field data. Using the FEM data of the optimized model, the team performed RNT prediction to understand how the performance of the NN model developed as a result of Tasks 6 and 7 is affected by rail geometry. The same NN architecture was employed. And the input dataset was divided into training (70%), validation (15%), and testing subsets (15%). And the NN performance for predicting RNT from input data was evaluated with testing data, as shown in Figure 29. RNT predictions resulted from resonance frequencies of 31, 37, and 39 kHz are perfectly aligned with the target performance, which confirms the feasibility of using NN and cross-sectional modes for RNT prediction on a different rail size.

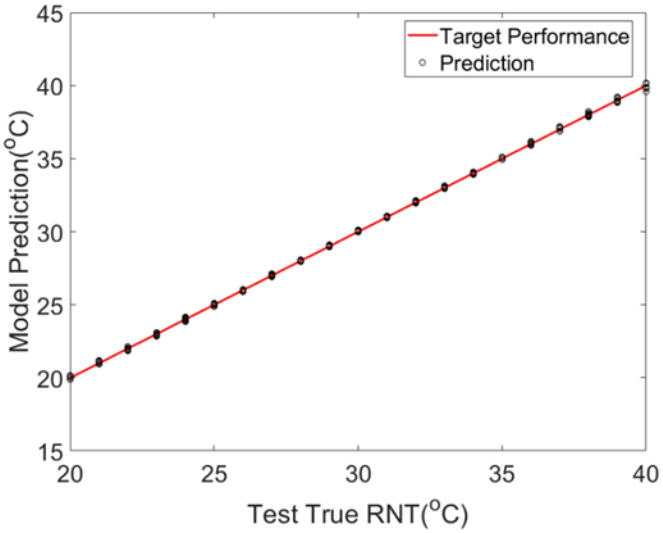

Figure 29: RNT prediction results using FEM data on a standard 132RE rail

Plans for Implementation

The project investigators developed the acoustic rail track vibration measurement system and machine learning algorithms for RNT prediction, and successfully demonstrated its feasibility through field tests. The next step is to improve system performance to the target accuracy of ±5ºF before taking it for commercialization. Throughout this study, the team has demonstrated that the cross-sectional vibrational modes are immune to boundary condition variations and sensitive to both temperature and axial loads. By modeling the cross-sectional modes with thermal loads, it is feasible to estimate RNT with acceptable accuracy. However, errors led by field measurements or FEM can negatively impact their performance. On the other hand, cross-sectional modes at a higher frequency range (>70 kHz) come with higher sensitivities to axial load and RNT, as shown in Figure 23(a). The higher the sensitivity to RNT, the more accurate the RNT prediction can be. The reason is that the RNT sensitivity from resonances of 31, 37, and 39 kHz are comparable or sometimes smaller than measurement/model errors. With improved RNT sensitivity, it is highly likely that sensitivity to RNT from higher frequency modes will be significantly distinguishable from model errors. Therefore, the team will investigate the experimental setup, which can efficiently promote desirable cross-sectional modes. For example, the current setup promotes a vibrational mode of 37 kHz, which demonstrates a good signal-to-noise ratio and low uncertainty for measurements. Modes such as resonances at 41, 49, and 60 kHz can be observed but not consistently. Rather than using a metallic impactor, piezoelectric transducers can be attached to a rail at different locations of rail cross-section to promote vibrational modes at a higher frequency range. This work includes laboratory testing for technology development and field data collection on revenue-service lines for technology validation and evaluation.

Upon successful completion of the proposed work, the team will reach out to BNSF to demonstrate the methodology and share the developed techniques, methodologies, and results with them for potential implementation in their maintenance practice. We believe that appropriate training about the method and approach will be beneficial for interested users. Where possible, we will collect actual data from various different rail sections to check the NN model. In addition, the results and methodologies will be presented in national conferences, published in national newsletters and journals for a broader outreach.

Finally, the project investigators will post the machine learning prediction framework as a benchmark for the NDE community in a computer code-sharing site such as Github.

Conclusions

This study explored an innovative approach for stress state, or RNT, prediction of CWR using contactless acoustic sensing and machine learning methods. An impulse-based experimental device was designed and deployed to excite multiple vibrational modes in rail simultaneously at one time. The device was tested in the laboratory on a short piece of rail (24 in) to evaluate the equipment and then to understand the influence of stress and temperature on the acoustic response. Then, the team coordinated with our rail industry partner, BNSF, and established a field test site on a revenue-service line in the state of Illinois. The test site was instrumented to support real-time data logging and streaming of rail temperature, longitudinal strain and load, RNT, and air temperature. The team collected acoustic vibration data from the rail at the instrumented test site during six separate visits throughout the summer and fall seasons, which cover a wide range of temperature and thermal stress conditions. The data revealed a set of vibrational modes that demonstrated predominant sharp resonance peaks within the ultrasonic frequency range. The character of the excited modes and the stress response of the vibration data from the field test site were notably different from those obtained from our laboratory tests. First, the dynamic response of a short piece of rail subject to an impact event is dominated by flexural, axial, torsional, and coupled vibrational modes that are set up by reflections from the rail ends and cross-sectional geometry. On the other hand, CWR, with its long length, tends to excite modes whose energy couple into the cross-section and do not transmit away from the excitation cross-section. Thus, we conclude that actual thermal stress and acoustic conditions of actual in-service CWR are very different from a finite length of rail tested in the laboratory, and the latter is probably not sufficient to represent realistic track conditions. Thus, future studies should focus on data collected from well-instrumented CWR track sections.

The cross-sectional modes generated in long length rail are generally insensitive to underlying boundary conditions such as tie condition and spacing, fastener and clip condition and position, and sub-base variations. These characteristics make cross-sectional modes good candidates for longitudinal load or RNT measurement of the rail itself. Although the frequencies of these cross-sectional vibrational modes are affected by temperature-induced stress in CWR structures, they exhibit complex and coupled behavior under temperature and longitudinal load variations. With the help of FEM simulations, the team investigated the behavior of cross-sectional modes under the influence of mechanical and thermal loads. The numerical models confirm mode-dependent sensitivity to stress and rail temperature. Based on the dataset obtained from the field test site, a group of cross-sectional modes with resonance frequencies of 31, 37, and 39 kHz were identified as suitable candidates to study with respect to detectability and reliability. Using the results from the FEM and employing a neural network, the team performed a regression analysis to predict RNT from the frequency data of those selected cross-sectional modes. The results suggest that the stress sensitivities of those particular cross-sectional modes are not sufficient to support RNT prediction with a target accuracy consistently within ±5ºF. However, NN analysis based on higher frequency cross-sectional modes can support RNT prediction with satisfactory accuracy. In particular,

FEM data analysis illustrated that a group of cross-sectional modes with resonance frequencies above 70 kHz would be more suitable candidates for RNT prediction because of improved stress sensitivity. In summary, we believe that RNT prediction using acoustic resonance modes has great potential and can be improved by (i) selecting modes with high stress sensitivity; (ii) establishing modal temperature sensitivity; and (iii) employing appropriate FE model accuracy.

In order to move this work forward toward practical implementation, future research on rail stress determination using vibration modes shall focus on effective cross-sectional modes generation using piezoelectric transducers to promote vibrational modes at higher frequency range and developing appropriate high-fidelity and efficient FE models for those high-frequency modes, and continuing to use data collected from instrumented actual rail structures. Practical issues such as different rail wear conditions, curved track, and varying boundary conditions that must be considered for large-scale deployment. The case of tie-to-tie variations is especially interesting because they could change the vibration-RNT relationship at the specific rail location, but also because they could change the "relevance zone" of an RNT measurement, that is how many ties would have to be accounted for to properly predict a representative RNT value for a given rail location. Many of these issues can be well studied using appropriate FEM simulations.

References

1. A. Kish, S. Kalay, A. Hazell, J. Schoengart, and G. Samavedam. *Rail Longitudinal force measurement evaluation studies using the track loading vehicle*. AAR report, 1993.
2. T.P. Boggs, J.G. Be´ liveau, and T.M. Murray. *Determination of axial load and support stiffness of continuous beams by vibration analysis*. AAR Research Report, No. CE/VPI-ST 94/14, 1994.
3. V. Damljanović and R.L. Weaver. Laser vibrometry technique for measurement of contained stress in railroad rail. *Journal of sound and vibration*, 282, No. 1-2, pp. 341-366.
4. C. Prada, O. Balogun, and T. W. Murray. Laser-based ultrasonic generation and detection of zero-group velocity Lamb waves in thin plates. *Applied Physics Letters*, 87, No. 19 2005, 194109.
5. F. Chen and P.D. Wilcox. The effect of load on guided wave propagation. *Ultrasonics*, 47, No. 1-4, 2007, pp. 111-122.
6. H. J. Lim and H. Sohn. Online Stress Monitoring Technique Based on Lamb-wave Measurements and a Convolutional Neural Network Under Static and Dynamic Loadings. *Experimental Mechanics*, 60, No. 2, 2020, pp. 171-179.
7. Bartlett, P.L. and Maass, W., 2003. Vapnik-Chervonenkis dimension of neural nets. *The handbook of brain theory and neural networks*, pp.1188-1192.